Integral Sliding Mode Control for a Marine Growth Removing ROV with Water Jet Disturbance

Benzon, Malte Severin Rosencrone von; Sørensen, Fredrik Fogh; Liniger, Jesper; Pedersen, Simon; Klemmensen, Sigurd; Schmidt, Kenneth

Published in:
2021 European Control Conference (ECC)

DOI (link to publication from Publisher):
10.23919/ECC54610.2021.9655050

Publication date:
2021

Document Version
Accepted author manuscript, peer reviewed version

Integral Sliding Mode Control for a Marine Growth Removing ROV with Water Jet Disturbance**

Malte von Benzon †*, Fredrik Sørensen†, Jesper Liniger†, Simon Pedersen†,
Sigurd Klemmensen§, Kenneth Schmidt†
†Department of Energy Technology, Aalborg Univerity, Esbjerg, Denmark
§SubC Partner A/S, Esbjerg, Denmark
*Corresponding author email: msrvb@et.aau.dk

***Abstract*—Oil & gas operators spend tens of million USD every year on removing marine growth, using manually operated remotely operated vehicles (ROV) with water jets. This study investigates the benefits of automating the ROV used for cleaning by demonstrating a sliding mode control (SMC) algorithm on a reconfigured BlueROV2 with an attached water jet. A nonlinear SMC was designed for the cleaning task. SMC was able to stabilize the orientation of the ROV while following a trajectory in depth. Regular SMC could not stabilize the ROV in front of the member, with the water jet activated. To accommodate for the delay, integral action was added to the SMC (IxSMC) in the surge direction, which stabilized the ROV. From the research presented in this paper, it can be concluded that automation of a marine growth removing ROV can be achieved by applying IxSMC.**

Keywords Sliding Mode Control, Integral Control, Underwater Robotics, ROV, Offshore Robotics, Nonlinear Control, Near-structure Operation, BlueROV2

I. Introduction

Marine growth increases the circumference and weight of underwater structures, increasing the hydrodynamic loads and gravity force. A typical layer of marine growth in the North Sea increases hydrodynamic loads by 17.5% and the weight by 0.15% [1]. The increased loads significantly increase material fatigue, and thereby the lifespan of the structures is potentially reduced. Today marine growth is either cleaned off by manually operated ROVs or handled by over-sizing the structures. The offshore industry suspects that automation of the ROVs will greatly reduce the cost of operation [2, 3, 4].

Manually operated ROVs, performing a task are hard to control due to the force from the cleaning tool. [5, 6]. The control algorithms for industrial ROVs are centered around controlling the manipulator [6], and thereby the operator still has an active role in controlling the ROV. Automatic cleaning off sub-sea structures requires good trajectory tracking and disturbance rejection. Different control algorithms have been used for ROVs concerning these objectives, some of which are based on model predictive control (MPC) [7, 8] or sliding mode control (SMC) [9, 10, 11]. MPC offers better overall performance compared to SMC. However, the heavy online computational requirement is the main difficulty of MPC since ROVs' computational capacity is often limited [8]. Several SMC schemes have been used to either control robotic arms attached to ROVs or to compensate for the force applied to the ROV by a robotic arm [6]. In [9] an SMC is designed to reject model uncertainties and disturbances from a robotic arm onto an ROV. Thus, this study examines SMC for trajectory tracking while cleaning a sub-sea structure using a water jet.

The contribution of this paper is the investigation of near-structure autonomous operation by designing a controller for a marine growth removing ROV. The controller will be based on SMC and experimentally validated on a reconfigured BlueROV2. The nonlinear SMC will be compared to a typical linear quadratic regulator with integral action(LQRI). This paper presents a description of the reconfigured ROV and test setup in section II, a mathematical model of the ROV is developed in section III. The SMC is designed in section IV and tested in section V.

II. Platform and test setup

In this paper, the marine growth removal process is simplified to water jetting of cylindrical members e.g., vertical jacket members, and mono-piles. Water jetting is commonly used for marine growth removal in the industry.

A. Reconfiguration of BlueROV2

The ROV used in this research is based on the BlueROV2 provided by Blue Robotics inc. The BlueROV2 has been reconfigured with the Heavy upgrade kit, enabling motion control in all six degrees of freedom. The ROV configuration is seen in Fig.1(a). A water jetting tool is installed; this can be seen in Fig. 1(c). The high-pressure water is provided from the topside by a pump and is delivered to the ROV through a high-pressure water hose. A mount is added(shown in Fig. 1(f)) to secure the hose and tether close to the center of mass of the ROV; this is done to minimize the effect on the ROV.

B. Sensors

The BlueROV2 is equipped with an accelerometer, a gyroscope, and a pressure sensor for attitude and depth measurement.

**This work was supported by Siemensfonden

The accelerometer and gyroscope are experimentally calibrated based on [12], and the magnetometer is both hard- and soft-iron calibrated based on [13]. A short baseline (SBL) underwater positioning system from WaterLinks was used. The locator from this is shown in Fig. 1(e). The SBL system has a constant delay of 1.2 sec; A similar delay has been found by [14] in the same SBL system. Due to the large delay, the SBL system has only been used to validate the mechanical model.

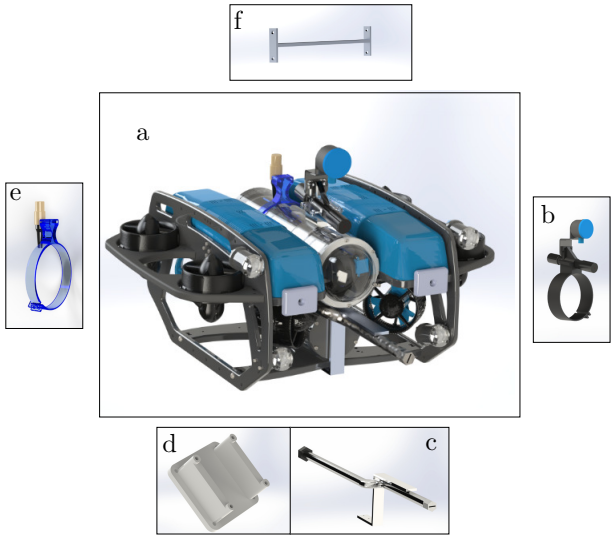

Fig. 1. The additional equipment added to BlueROV2 Heavy configuration.

A relative distance measurement from ROV to the structure is facilitated by a laser pointer and a camera on the ROV, as inspired by [15]. The laser is mounted at an angle to the camera's direction of view and is seen in Fig. 1(b). The distance can be determined by tracking the laser dot's vertical position in the image. The distance algorithm exhibits a constant delay of 0.4 sec when implemented on the Raspberry Pi 3 installed on the BlueROV2. A similar algorithm using the same camera and laser was developed to obtain the sway position relative to the structure. However, due to limited computational power on the BlueROV2, it has not been possible to implement sway feedback.

In Tab.I, an overview of the sensors is given. To distinguish between BlueROV2 and the upgraded BlueROV2 used in this project, the ROV used in this project will be referred to as BlueROV2 CC (cleaning configuration).

Tab. I. Sensor characteristics.

Sensor	Sampling Rate	Noise (Variance)	Delay
IMU	20 Hz	2.5×10^{-5} rad	-
Pressure Sensor	20 Hz	1.5×10^{-5} m	-
SBL	4 Hz	1.3×10^{-3} m	1.2 sec
Laser camera sensor	20 Hz	2×10^{-6} m	0.4 sec

III. Mechanical Model

A. ROV model

The mechanical model of the ROV is derived based on [16]. The model of BlueROV2 CC is seen in (1) and (2). The reference frame used in this research is shown in Fig. 2.

$$\dot{n} = J(n)v \tag{1}$$

$$\mathbf{M}\dot{\mathbf{v}} + \mathbf{C(v)v} + \mathbf{D(v)v} + \mathbf{g(n)} = \boldsymbol{\tau_t} + \boldsymbol{\tau_{jet}} \tag{2}$$

The different variables of (2) can be seen in Tab. II, except for **g(n)** and **C(v)** which are the gravitational/buoyancy force and Coriolis/centripetal forces respectively. $\boldsymbol{\tau_{jet}}$ is the force from the water jet, acting in the surge direction. A description of these can be found in [16, 8]. The BlueROV2 CC is neutrally buoyant and assumed to rotate around the center of mass. The physical parameters of the BlueROV2 CC are shown in Tab. III.

Tab. II. Parameters and states for the BlueROV2 CC model.

Description	Variable	Components	Size
Mass matrix	**M**	$\mathbf{M_{RB}} + \mathbf{M_a}$	6x6
Mass/Inertia	$\mathbf{M_{RB}}$	$\text{diag}(m\ m\ m\ I_x\ I_y\ I_z)$	6x6
Added Mass/Inertia	$\mathbf{M_a}$	$\text{diag}(m_{a,x}\ m_{a,y}\ m_{a,z}\ I_{a,x}\ I_{a,y}\ I_{a,z})$	6x6
Thruster force	$\boldsymbol{\tau_t}$	$(f_x\ f_y\ f_z\ \tau_\phi\ \tau_\theta\ \tau_\psi)^T$	6x1
Body frame velocity	**v**	$(\dot{x}\ \dot{y}\ \dot{z}\ p\ q\ r)^T$	6x1
Form drag	**D**	$(f_{d,x}\ f_{d,y}\ f_{d,z}\ \tau_{d,\phi}\ \tau_{d,\theta}\ \tau_{d,\psi})^T$	6x1

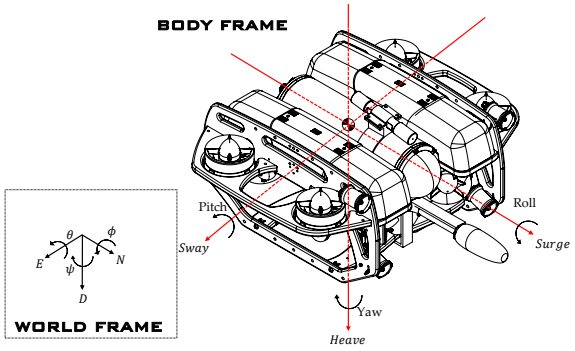

Fig. 2. The reference frame used for analysis of BlueROV2 CC.

Tab. III. Constants for the BlueROV2 CC model.

Description	Parameter	Value	Unit
Mass	m	13.50	kg
Moment of inertia	I_{xx}, I_{yy}, I_{zz}	$0.26, 0.23, 0.37$	kgm^2
Dimensions	L, H, W	$0.46, 0.38, 0.58$	m
Volume	$\mathcal{V}$	0.0134	m^3
Distance from center of mass to center of buoyancy	r_g^b	0.01	m
Gravity acceleration	g	9.82	$\frac{m}{s^2}$
Water density	ρ	1000	$\frac{kg}{m^3}$

An estimate of the added mass matrix for the BlueROV2 CC is found based on [17]. The added mass matrix is shown in (3).

$$\mathbf{M}_a = diag\left(6.36, 7.12, 18.68, 0.189, 0.135, 0.222\right) \tag{3}$$

The drag force **D** is found by flow simulations in SolidWorks® Flow Simulation which is an embedded program in SolidWorks®. The results are corrected by experiments, similar to the approach in [14]. The result is shown in Tab. IV.

Tab. IV. Corrected drag force/torque eqns.

Motion	Drag force/torque	R^2
Surge	$f_{d,x} = 141\|\dot{x}\|\dot{x} + 13.7\dot{x}$	0.98
Sway	$f_{d,y} = 217\|\dot{y}\|\dot{y}$	0.99
Heave	$f_{d,z} = 190\|\dot{z}\|\dot{z} + 33\dot{z}$	0.99
Roll	$\tau_{d,\phi} = 1.19\|p\|p$	0.94
Pitch	$\tau_{d,\theta} = 0.47\|q\|q + 0.8q$	0.94
Yaw	$\tau_{d,\psi} = 1.9\|r\|r$	0.95

B. Water Jet Model

A finite control volume momentum analysis is carried out to determine the force acting on the BlueROV2 CC from the high-pressure water jet. The water jet's transient response is neglected; therefore, the water jet can be assumed to be in a steady-state. Furthermore, due to the constant temperature and relatively low pressure(100-500 bar), water density can be assumed to be constant. The water jet used in this project produces 16.6 N force($\boldsymbol{\tau_{jet}}$) with a flow rate of 8.3 $\frac{L}{min}$. This can approximately be scaled (by a linear scale concerning a ratio between maximum thrust and mass) to an industrial ROV(M500) for marine growth removal with a flow rate of 25 $\frac{L}{min}$ at 250 bar, which is a normal cleaning flow according to operators in the North Sea.

C. Thruster

There are eight T200 thrusters installed on BlueROV2 CC. The input to force curve for two thrusters has been derived in [14], these results will be used in this study. The transient response of the thrusters has been found by identifying an auto-regressive exogenous(ARX) model in MATLAB® on data provided by MathWorks®[18]. The continuous transfer function describing the transient from input to output force is given by (4). The transfer function has been neglected in the control design due to the thruster dynamics being magnitudes faster compared to the ROV dynamics. The thruster dynamics has been implemented in the simulations. The maximum velocities of the vehicles for each direction of motion are seen in Tab. V.

$$\frac{F(s)}{U(s)} = \frac{6136s + 108700}{s^3 + 89s^2 + 9258s + 108700} \tag{4}$$

Tab. V. Maximum velocities in body frame.

Movement body frame	Maximum velocity
$\dot{x}_{max}$	0.72 $\frac{m}{s}$
$\dot{y}_{max}$	0.63 $\frac{m}{s}$
$\dot{z}_{max}$	0.71 $\frac{m}{s}$
p_{max}	5.2 $\frac{rad}{s}$
q_{max}	4.9 $\frac{rad}{s}$
r_{max}	3.6 $\frac{rad}{s}$

IV. Controller Design

A. Design of Sliding Mode Controller

Controllers will be designed based on SMC for each direction of motion decoupled, thereby cross-coupling is not taken in to consideration in the control design. The book [19] is used as a reference to design the SMC. The controller will be designed concerning the body frame. In this section, variables will be denoted x to indicate that it belongs to the surge motion. The equation for the surge motion can be formulated as seen in (5), by making the simplifications seen in (6) and (7).

$$\ddot{x} = K_x + h_x f_x \tag{5}$$

$$K_x = -(\frac{C_x(\mathbf{v})\mathbf{v} + g_x(\theta) - \tau_{jet}}{m + m_{a,x}}) \tag{6}$$

$$h_x = \frac{1}{m + m_{a,x}} \tag{7}$$

B. Stability Analysis of Controller for Surge

The time varying surface σ_x is defined by (8). The error between the state (x) and the reference (r_x) is given by (9). $c_{0,x}$ is a positive integer that ensures stability of σ_x. The error dynamics is given by (10). $\sigma_x = 0$ is the sliding surface, the idea is now to design a controller which keeps σ_x on the sliding surface after convergence.

$$\sigma_x = \dot{e}_x + c_{0,x}e_x \tag{8}$$

$$e_x = x - r_x \tag{9}$$

$$\dot{e}_x = \dot{x} - \dot{r}_x \tag{10}$$

σ_x needs to reach the sliding surface within finite time using f_x under the influence of the system and the disturbance, described by K_x. The input f_x can be designed using Lyapunov analysis to ensure that the sliding surface can be reached along the system trajectories within finite time $\sigma_x \to 0$ for $t \to t_r < \infty$. The Lyapunov function in (11) is used.

$$V(\sigma_x) = 0.5\sigma_x^2 \tag{11}$$

To ensure global asymptotic stability $V(\sigma)$ must be positive definite $V(\sigma) \to \infty$ for $\sigma \to \infty$ and $\dot{V}$ must be negative definite $\dot{V}(\sigma) < 0 \ \forall \ \sigma \ \neq 0$. $\dot{V}$ is bounded, which can be expressed as (12).

$$\dot{V}(\sigma_x) = -\alpha_x\sqrt{V(\sigma_x)} \tag{12}$$

$\alpha_x > 0$, which can be proven by separation of variables, thereby t_r is finite and dependent on the value α_x and the initial error of the position and velocity, as long as the derivative of (11) is upper bounded by (12). Then the derivative of (11) is decrescent and since (12) is negative definite $\sigma_x = 0$ is finite-time stable. The control law can be found by applying these conditions. The time derivative of (11) is seen in (13).

$$\dot{V}(\sigma_x) = \sigma_x\dot{\sigma_x} \tag{13}$$

Inserting (8) in (13) leads to (14).

$$\dot{V}(\sigma_x) = \sigma_x(K_x + h_x f_x - \ddot{r_x} + c_0\dot{e}_x) \tag{14}$$

Choosing f_x to be (15).

$$f_x = \hat{h}_x^{-1}(\ddot{r_x} - c_{0,x}\dot{e}_x + b_{in}) \tag{15}$$

where $\hat{h}_x$ is the model estimate of h_x and b_{in} is the control term, (14) then becomes (16).

$$\dot{V}(\sigma_x) = \sigma_x(K_x + h_x(\hat{h}_x^{-1}(\ddot{r_x} - c_{0,x}\dot{e}_x + b_{in})) - \ddot{r_x} + c_{0,x}\dot{e}_x) \tag{16}$$

Assuming that $\hat{h}_x = h_x$, (16) becomes (17).

$$\dot{V}(\sigma_x) = \sigma_x(K_x + b_{in}) \tag{17}$$

Furthermore, K_x is bounded by an upper value $L_{b,x}$ (18), since both the dynamics of the ROV and the disturbance are bounded.

$$L_{b,x} \geq K_{x,max} \tag{18}$$

$K_{x,max}$ is found by inserting the maximum velocity Tab. V in the equation of motion (5). The disturbance force is the water jet force. Thereby (17) can be written as (19).

$$\dot{V}(\sigma_x) = \sigma_x(K_x + b_{in}) \leq |\sigma_x|L_{b,x} + |\sigma_x|b_{in} \tag{19}$$

b_{in} is chosen to be (20).

$$b_{in} = -\rho_s sgn(\sigma_x) \tag{20}$$

$$sgn\,(\sigma_x) = \begin{cases} 1, & \sigma_x > 0 \\ -1, & \sigma_x < 0 \end{cases}, sgn\,(0) \in [-1, 1] \tag{21}$$

ρ_s is a gain which can be chosen based on (12) and (19) shown in (22).

$$\dot{V}(\sigma) \leq |\sigma_x|(L_b + \rho_s) = -\alpha_x\sqrt{V(\sigma_x)} \tag{22}$$

Inserting (11) in (22) shown in (23).

$$\rho_s = L_{b,x} + \frac{\alpha_x}{\sqrt{2}} \tag{23}$$

There are now two tuning parameters, $c_{0,x}$ and α_x, which ensure stable convergence of the sliding surface. In practice, L_b can also be tuned. To avoid chatter in the input the sign function in (20) is approximated by a Sigmoid function defined in (24). Thereby the controlled system error is bounded in a boundary layer in the neighborhood close to the sliding surface. This approximation introduces another tuning parameter $\epsilon_{s,x}$ which is a positive value and has a relationship to the thickness of the boundary layer.

$$sgn(\sigma_x) \approx \frac{\sigma_x}{|\sigma_x| + \epsilon_{s,x}} \tag{24}$$

SMC controllers have been designed for each direction of motion.

The implemented controller is shown in (25).

$$f_x = h_x^{-1}(\ddot{r_x} - c_{0,x}\dot{e} + \rho_s\frac{\sigma_x}{|\sigma_x| + \epsilon_{s,x}}) \tag{25}$$

C. Integral Action for Surge Motion

It has not been possible to tune an SMC controller to stabilize the surge motion when the water jet was turned on. The delay in the distance measurement causes instability. To cope with this an integral part was added to the sliding mode controller based on [20]. A similar approach to integral sliding mode control(ISMC) has been used in [21] to obtain accurate position tracking. ISMC introduces a new tuning parameter $K_{i,x}$ which must be positive. Thereby a less aggressive controller can be designed since the integral part limits the water jet effect.

An ISMC was designed by splitting the control function $b_{in,I}$ into two terms seen in (26).

$$b_{in,I} = b_{in,1} + b_{in,2} \tag{26}$$

$b_{in,1}$ is the auxiliary control that compensates for the bounded disturbance and is designed in such a way that the sliding starts immediately, and $b_{in,2}$ is driving the sliding variable towards zero as time increases [20]. $b_{in,1}$ can be found from the new sliding variable (27) and dynamics (28), by following the same procedure which led to (20). $b_{in,1}$ is seen in (29).

$$\begin{cases} S_x = \sigma_x - J_x \\ \dot{J}_x = -b_{in,2} \end{cases} \tag{27}$$

$$\dot{S}_x = K_x + h_x f_x - (b_{in,1} + b_{in,2}) - (-b_{in,2}) \tag{28}$$

$$b_{in,1} = -\rho_s sgn(S_x) \tag{29}$$

Thereby the original sliding variable dynamics can be written as (30).

$$\begin{aligned} \dot{\sigma}_x &= K_x + h_x f_x - b_{in,1} - b_{in,2} \\ \dot{S}_x &= K_x + h_x f_x - b_{in,1} \end{aligned} \tag{30}$$

Then $\dot{\sigma}_x$ can be described in auxiliary sliding mode by making $\dot{S}$ = 0 and finding the $b_{in,1,eq}$ done in (31). This leads to (32).

$$0 = K_x + h_x f_x - b_{in,1,eq} \Rightarrow b_{in,1,eq} = K_x + h_x f_x \tag{31}$$

$$\dot{\sigma}_x = -b_{in,2} \tag{32}$$

As explained in [20] the control function $b_{in,2}$ can be chosen as (33)

$$b_{in,2} = k_{i,x}\sigma_x,\ k_{i,x} > 0 \tag{33}$$

$k_{i,x}$ is the convergence rate of the sliding variable. A Sigmoid function once again approximates the sign function in (29), hereby the new control function becomes (34).

$$b_{in,I} = -k_{i,x} \cdot \sigma_x - \rho_s\frac{(S_x)}{|S_x| + \epsilon_{s,x}} \tag{34}$$

As seen in (28), S_x is a function of J_x, which is found by integration of $\dot{J}_x$. At the initial moment $J_x = \sigma(0)$. The implemented surge controller based on ISMC is shown in (25).

$$f_{x,i} = h_x^{-1}(\ddot{r_x} - c_{0,x}\dot{e} + b_{in,I}) \tag{35}$$

SMC has been designed for the remaining directions of motion based on section IV-B, to clarify the combined controlled system will be referenced as IxSMC.

D. Tuning of Control Parameters

The various control parameters covered in section IV-A has been tuned through simulations and experiments in the test facility. The tuned control parameters are shown in Tab. VI. $K_{i,x}$ has been chosen to be 1.5. It was found that the IxSMC was sensitive to the tuning parameters, especially the L_b gain, which represents the bounds of the system and the disturbance.

Tab. VI. Tuned control parameters for IxSMC.

Controller	α	C_0	ε_s	L_b
Surge	0.1	1	0.08	1.17
Sway	0.5	3	0.03	1.04
Heave	0.1	2	0.05	0.70
Roll	0.1	0.4	0.1	2.01
Pitch	0.1	0.4	0.1	2.01
Yaw	0.1	2	0.1	2.05

V. Experimental Results

In the following section, the results of the experiments performed in the test facility are presented. An LQRI controller has been designed for the BlueROV2 CC based on [14]. The LQRI and IxSMC controllers have been implemented on the BlueROV2 CC. The tests are compared to a simulation of the ROV, running the respective controllers.

A. Test Setup

The test facility consisted of a circular commercially available pool, which had a diameter of 6.1 m and a height of 1.15 m. Two different cylindrical pipes were placed in the test facility, representing a member of an offshore structure; the pipes were 350mm and 600mm. The members of offshore structures are 330-4000mm.

B. Simulations

The mechanical model derived in section III is implemented in Simulink® together with the controller developed in section IV and the LQRI controller. The sampling frequency, delay, and noise from the sensors are also implemented together with the thrusters' dynamics.

C. Results

The ROV were made to follow a trajectory in depth (z_{ref}) while keeping a fixed distance of 0.1 m to the member in the test facility. The trajectory in depth (z_{ref}) varied from 0.7 to 0.2 m(surface is 0 m) and with a velocity of 0.12 m/s. The reference to the angles were set to zero. The controller was assessed on the mean error between the measured value and the reference and the variation from the reference quantified by two standard deviations(2sd).

The two tests are shown in Fig. 3 (IxSMC) and 4 (LQRI). Both tests show that the BlueROV2 CC is kept at constant depth (z_{test}) for the initial phase. After the BlueROV2 CC has stabilized, the water jet is turned on, and the ROV starts to follow the trajectory. It is only the angle in yaw shown in Fig. 3 and 4 since the other two angles were kept zero by the controllers.

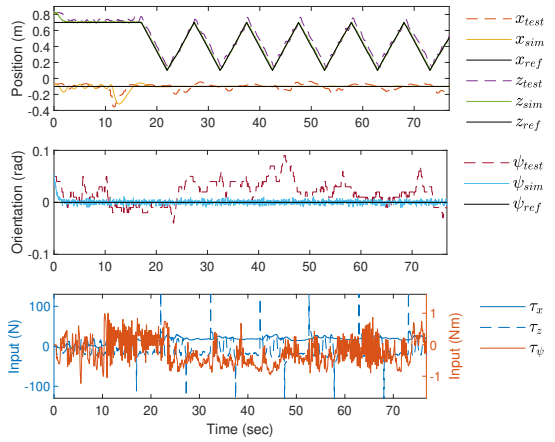

Fig. 3. IxSMC. References $x_r = -0.1\ m$, $z_r = variable(0.7 - 0.2m)$ and $\psi_r = 0\ rad$.

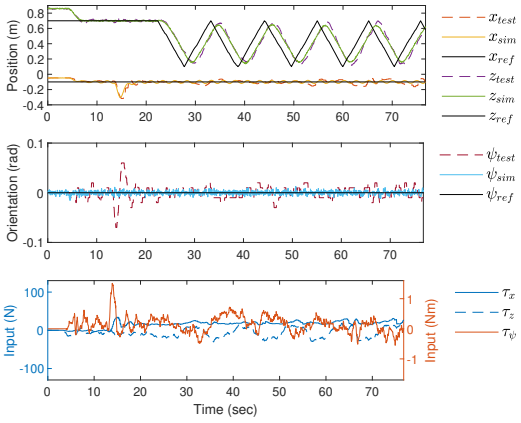

Fig. 4. LQRI. References $x_r = -0.1\ m$, $z_r = variable(0.7 - 0.2m)$ and $\psi_r = 0\ rad$.

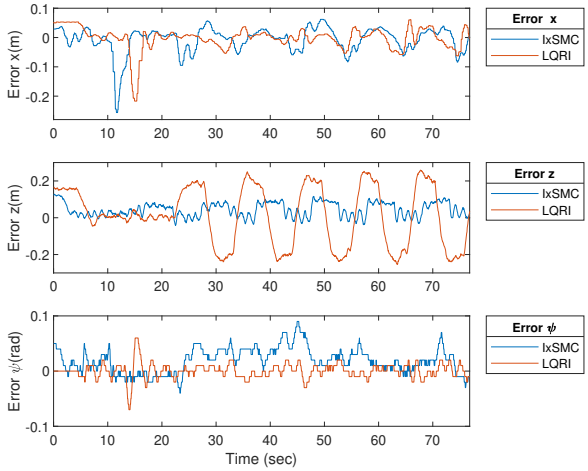

Fig. 5. Error comparison between IxSMC and LQRI , references $x_r = -0.1\ m$, $z_r = variable(0.7 - 0.2m)$ and $\psi_r = 0\ rad$.

In Fig. 5 a comparison between the two controllers are shown concerning the error in each direction of motion. In regards to the two constant references, ψ and x, the controllers are on par. In z the difference between the two controllers is more apparent as the LQRI can not keep up with

the varying reference, hence having a more significant error than IxSMC. Note that the errors between the two controllers can not be compared in terms of time due to the controllers not being started simultaneously.

The tests have been repeated three times in order to evaluate repeatability. The average results of the three tests for both controllers are seen in Tab. VII and VIII. Each test was similar to the results illustrated in Fig. 3 and 4.

Tab. VII. Average results of 3 tests with the LQRI controller.

Direction	Mean error	2sd of mean error
x	$-0.002\ m$	$0.046\ m$
z	0.007	$0.35\ m$
ψ	$0\ rad$	$0.02\ rad$

Tab. VIII. Average results of 3 tests with the IxSMC controller.

Direction	Mean error	2sd of mean error
x	$0\ m$	$0.072\ m$
z	$0.048\ m$	$0.09\ m$
ψ	$0.028\ rad$	$0.053\ rad$

VI. Conclusion and Future Work

This paper has presented the design and experimental validation of an ROV controlled by IxSMC and applied for near-structure high-pressure water jet cleaning. The controllers were implemented on a BlueROV2 reconfigured with a water jet for cleaning sub-sea structures. The controllers were experimentally examined for trajectory tracking while cleaning a cylindrical structure in a laboratory test facility. A comparison was made between IxSMC and LQRI for the application. Results show that the SMC controller could not stabilize the ROV when the water jet was activated. To accommodate for the delay, integral action was added to the SMC (IxSMC) in the surge direction, which stabilized the ROV. The tests were repeated three times. The control loop was limited to 20 Hz by the hardware on ROV. The experimental tests for both controllers showed consistency with the simulations which indicates that the model is suitable for the application.

The IxSMC controller followed the reference trajectory in depth with a mean error of $0.048\,\mathrm{m}$ with 2sd of $0.090\,\mathrm{m}$ compared to the LQRI controller, which had a mean error in depth of $0.007\,\mathrm{m}$ with 2sd of $0.35\,\mathrm{m}$. Thereby the SMC had a better trajectory tracking performance compared to LQRI. The IxSMC controller was able to keep a mean error between the reference and the measured distance to the structure of $0.00\,\mathrm{m}$ with 2sd of $0.072\,\mathrm{m}$. Results from the LQRI showed a mean error of $-0.002\,\mathrm{m}$ with 2sd of $0.046\,\mathrm{m}$. Conclusively, the two controllers' performance in terms of mean error is on par, while the LQRI yielded less variance in the control error. The IxSMC was able to keep the mean error of the angle ψ at $-0.01\,\mathrm{rad}$ with 2sd of $0.043\,\mathrm{rad}$. Compared to LQRI, which had a mean error of $0.00\,\mathrm{rad}$ with 2sd of $0.02\,\mathrm{rad}$. In term of mean error of the angle ψ were on par, while the IxSMC performed worse with regard to variance in the error.

Generally, the error of the IxSMC varied more compared to LQRI when the reference was kept constant. Regarding tracking a moving reference, the error of IxSMC varied less than LQRI. Both controllers' performance would be improved if the sample time were increased and the delay of 0.4 sec in the distance measurement was handled. It can be concluded that automation of a marine growth removing ROV can be achieved by applying IxSMC.

Further investigation is necessary to automate the marine growth removal process; this could include incorporating the environmental disturbances from waves and ocean current in the control design and thereby making it more robust for the application.

References

[1] T. Yan and W. X. Yan, "Fouling of offshore structures in china-a review," *Biofouling (Chur, Switzerland)*, vol. 19, no. sup1, pp. 133–138, 2003.

[2] E. Supply, "Ny undervandsrobot skal spare offshore-industrien for trecifret millionbeløb," 25. august 2020, in danish.

[3] I. Tena, "Automating rov operations in aid of the oil & gas offshore industry," Tech. Rep., August 2011.

[4] E. Research), "Acomar – auto compact marine growth remover," 2020, energiforskning.dk.

[5] T. W. McLain and S. M. Rock, "Experimental measurement of rov tether tension."

[6] S. Sivčev, J. Coleman, E. Omerdić, G. Dooly, and D. Toal, "Underwater manipulators: A review," *Ocean engineering*, vol. 163, pp. 431–450, Sep 1, 2018.

[7] L. V. Steenson, S. R. Turnock, A. B. Phillips, C. Harris, M. E. Furlong, E. Rogers, L. Wang, K. Bodles, and D. W. Evans, "Model predictive control of a hybrid autonomous underwater vehicle with experimental verification," *Proceedings of the Institution of Mechanical Engineers. Part M, Journal of engineering for the maritime environment*, vol. 228, no. 2, pp. 166–179, Feb 18, 2014.

[8] C. S. Chin and M. W. S. Lau, *Benchmark Models of Control System Design for Remotely Operated Vehicles*. Singapore: Springer Singapore Pte. Limited, 2020.

[9] G. V. Lakhekar and R. G. Roy, "Heading control of an underwater vehicle using dynamic fuzzy sliding mode controller." IEEE, Mar 2014, pp. 1448–1454.

[10] A. Alessandri, T. Hawkinson, A. J. Healey, and G. Veruggio, "Robust model-based fault diagnosis for unmanned underwater vehicles using sliding mode-observers," Tech. Rep., Aug 22, 1999.

[11] M. Eslami, C. S. Chin, and A. Nobakhti, "Robust modeling, sliding-mode controller, and simulation of an underactuated rov under parametric uncertainties and disturbances," *Journal of marine science and application*, vol. 18, no. 2, pp. 213–227, Jun 2019.

[12] S. Stančin and S. Tomažič, "Time- and computation-efficient calibration of mems 3d accelerometers and gyroscopes," *Sensors (Basel, Switzerland)*, vol. 14, no. 8, pp. 14 885–14 915, Aug 13, 2014.

[13] K. Winer, "Simple and effective magnetometer calibration," 15 Aug 2017.

[14] S. Pedersen, J. Liniger, F. F. Sørensen, K. Schmidt, M. von Benzon, and S. S. Klemmensen, "Stabilization of a rov in three-dimensional space using an underwater acoustic positioning system," *IFAC PapersOnLine*, vol. 52, no. 17, pp. 117–122, 2019.

[15] V. N. Kuhn, P. L. J. Drews Jr, S. C. P. Gomes, M. A. B. Cunha, and S. S. d. C. Botelho, "Automatic control of a rov for inspection of underwater structures using a low-cost sensing," *Journal of the Brazilian Society of Mechanical Sciences and Engineering*, vol. 37, no. 1, pp. 361–374, Jan 2015.

[16] T. I. Fossen, *Handbook of Marine Craft Hydrodynamics and Motion Control*, 1st ed. Hoboken: Wiley, 2011.

[17] O. A. Eidsvik, "Identification of hydrodynamic parameters for remotely operated vehicles," Ph.D. dissertation, Jun 10, 2015.

[18] M. C. F. Exchange, "Matlab and simulink robotics arena : From data to model," 14 Feb 2018.

[19] J.-J. E. Slotine and W. Li, *Applied Nonlinear Control*. Englewood Cliffs, NJ: Prentice Hall, 1991.

[20] L. Fridman, Y. Shtessel, C. Edwards, and A. Levant, "Sliding mode control and observation," Springer, Tech. Rep., 2014.

[21] M. M. Bech, H. C. Pedersen, T. O. Andersen, and L. Schmidt, "Sliding control with chattering elimination for hydraulic drives," *Applied mechanics and materials*, vol. 233, pp. 168–171, Nov 29, 2012.